ChemSusChem

Supporting Information

Bicarbonate Electroreduction to Multicarbon Products Enabled by Cu/Ag Bilayer Electrodes and Tailored Microenviroments

Jungkuk Lee, Hengzhou Liu, and Wenzhen Li*

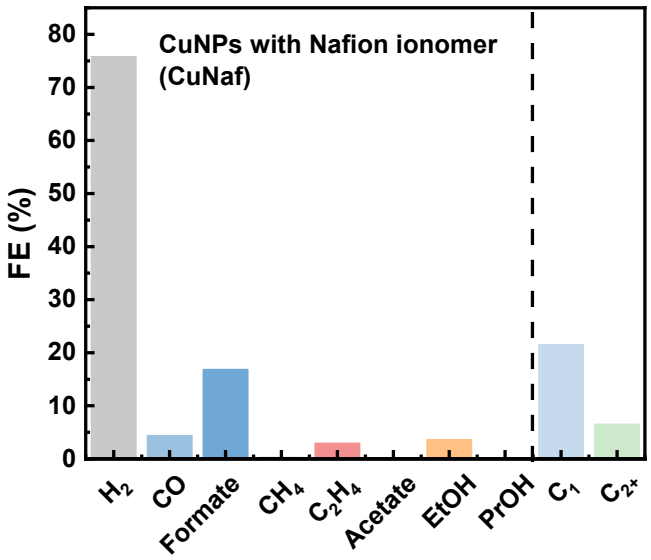

Figure S1. Product distributions of bicarbonate conversion of CuNaf catalyst on H23 carbon paper. The bicarbonate conversion was performed in MEA-based flow cell with BPM at a current density of 100 mA cm^{-2} for 1 h.

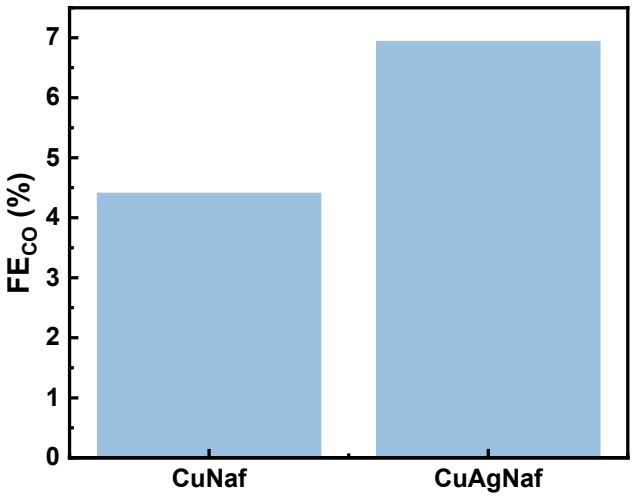

Figure S2. Comparison of FE_{CO} of CuNaf and CuAgNaf catalysts on H23 carbon paper. The bicarbonate conversion was performed in MEA-based flow cell with BPM at a current density of 100 mA cm^{-2} for 1 h.

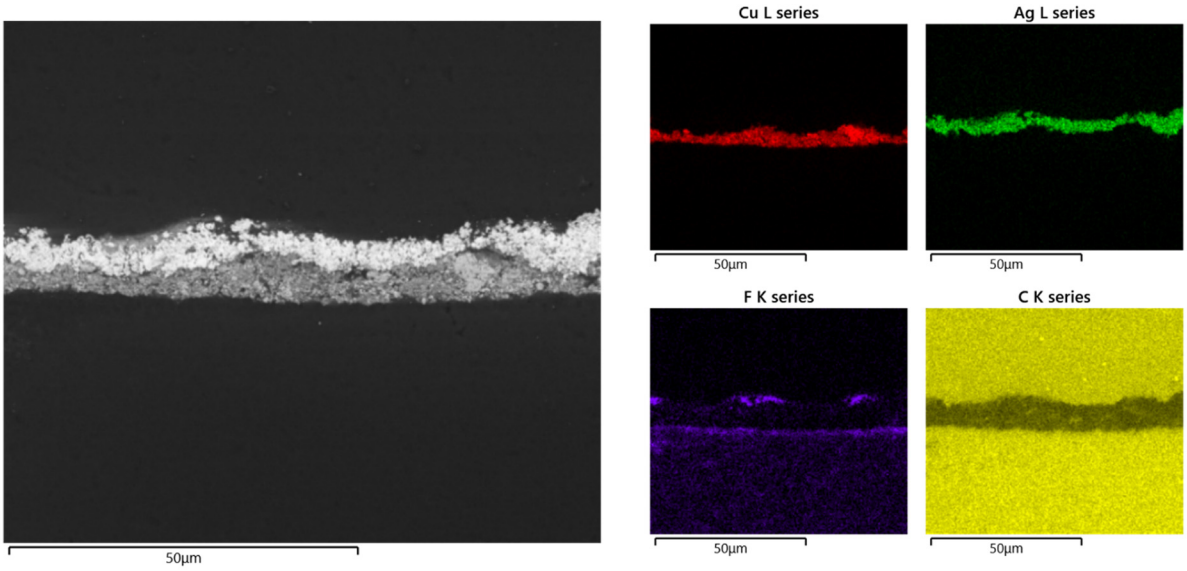

Figure S3. SEM image of bilayer CuSus/AgNaf electrode and corresponding EDX mapping. The carbon signal above the Ag layer is attributed to the epoxy matrix used for sampling.

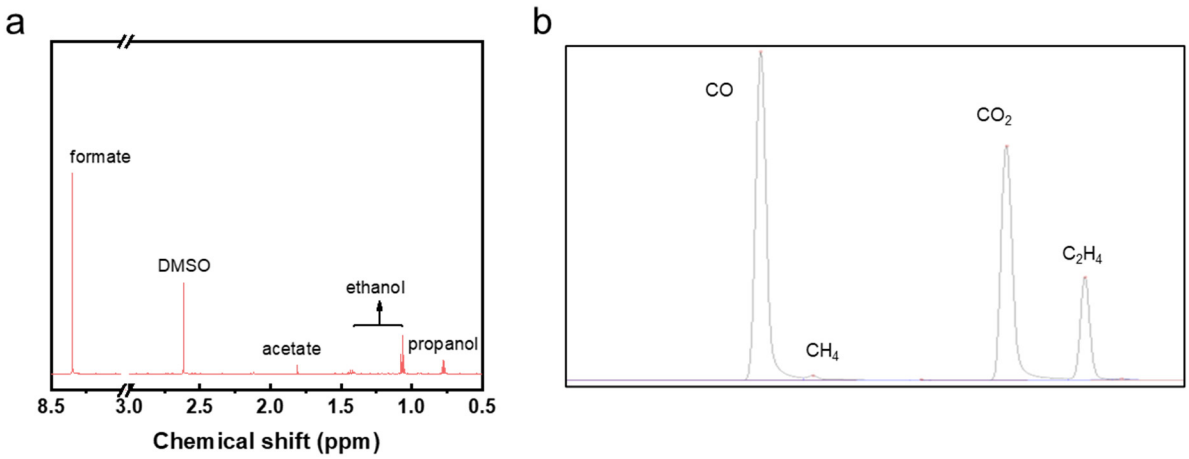

Figure S4. (a) ^{1}H NMR and (b) GC spectrum (FID signal) of the liquid and gaseous products, respectively.

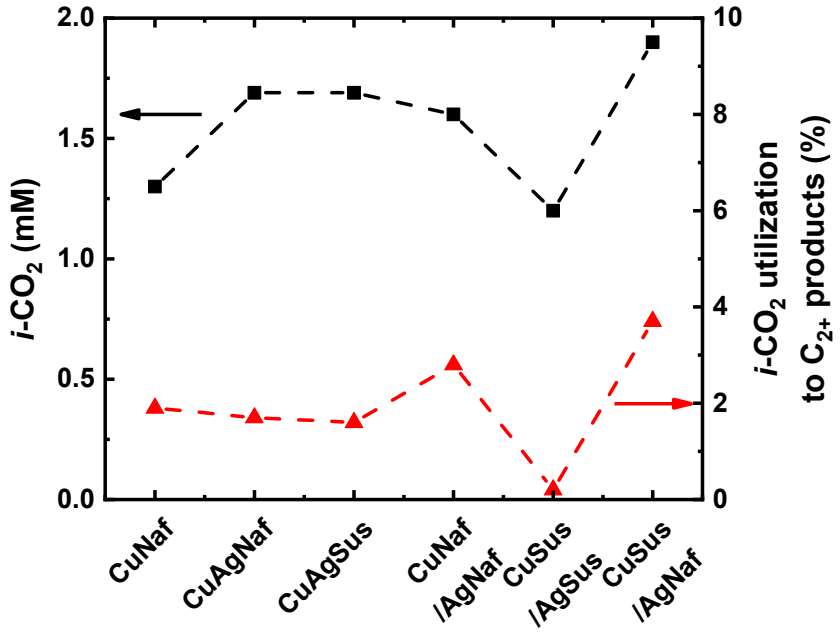

Figure S5. *i*-CO_2 formation and its utilization to C_{2+} products of six different electrode configurations during the bicarbonate conversion (100 $mAcm^{-2}$ for 1 h).

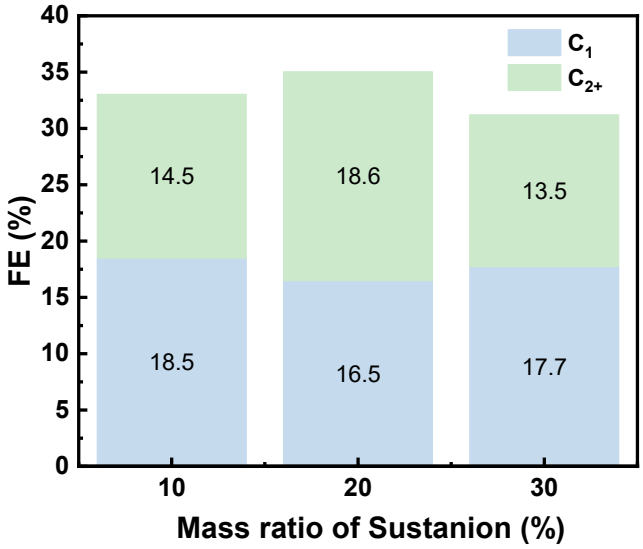

Figure S6. FE of C_1 and C_{2+} products as function of mass ratio of Sustanion on Cu layer. The Nafion content in Ag layer was maintained at 20 wt.%. The bicarbonate conversion was performed at a current density of 100 mA cm^{-2} for 1 h.

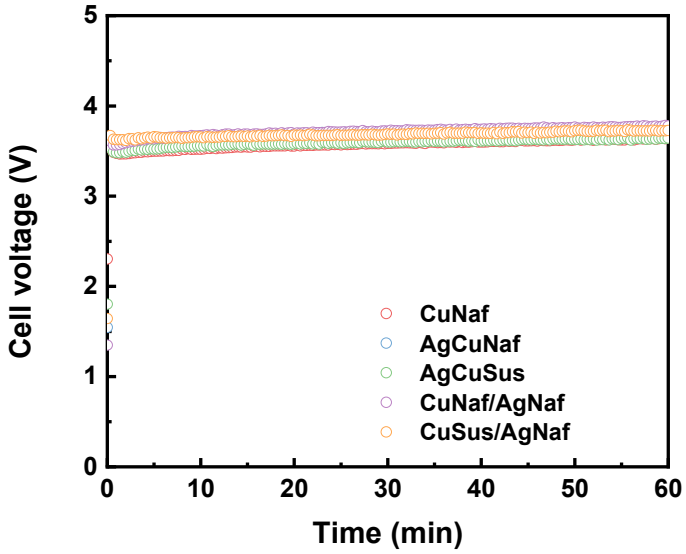

Figure S7. Cell voltage profiles of five different configurations of Cu and/or Ag catalysts with different ionomer (Nafion, Sustanion) on H23 carbon paper. The bicarbonate conversion was performed in MEA-based flow cell with BPM at a current density of 100 mA cm^{-2} for 1 h.

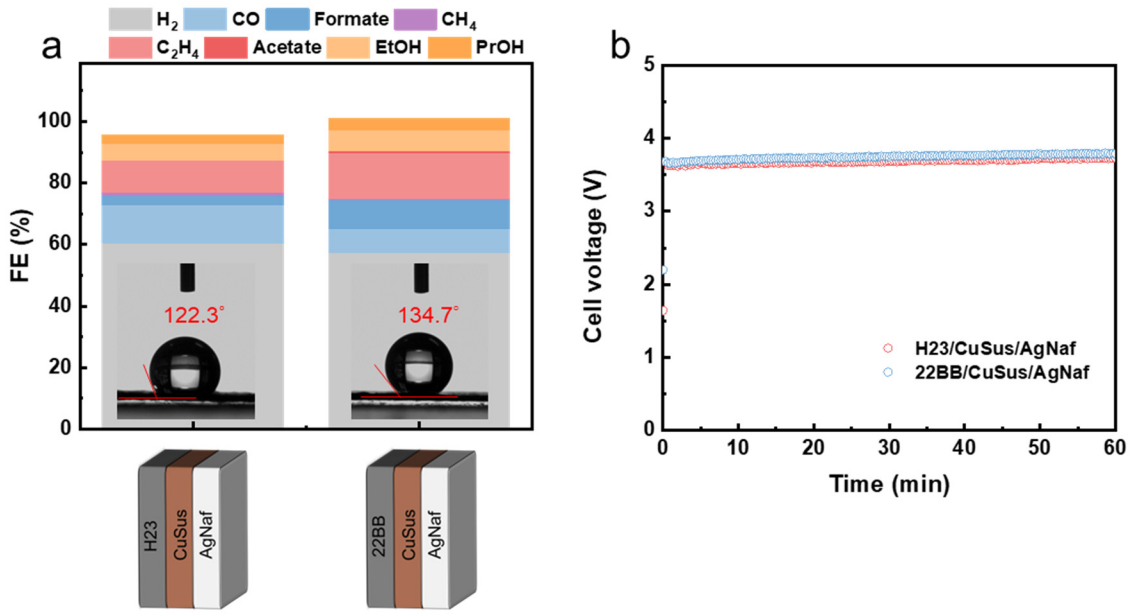

Figure S8. Comparison of (a) FE (inset: images of contact angle measurement on H23 and 22BB carbon paper without catalyst layer) and (b) cell voltages of bilayer CuSus/AgNaf electrode on H23 and 22BB carbon paper. The bicarbonate conversion was performed in MEA-based flow cell with BPM at a current density of 100 mA cm^{-2} for 1 h.

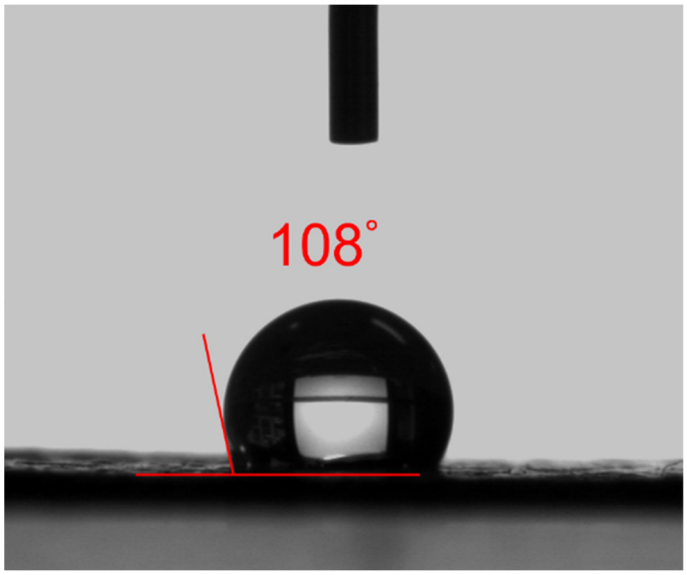

Figure S9. Contact angle measurement of CuSus/AgNaf-P50 after 1 h electrolysis.

Table S1. Comparison of eCO_2R performance of state-of-the-art coupled CO_2 capture and reduction systems.

Catalysts	CO_2 capture solution	Membrane	products	FE (%)	Current density (mA cm^{-2})	Cell voltages (V)	Ref
CuSus/AgNaf-p50	3 M $KHCO_3$	BPM	C_{2+}	41.6	100	3.9	This work
Cu nanoparticles	1 M K_2CO_3	BPM	C_{2+}	10.1	150	n/a	[1]
Cu foam	3 M $KHCO_3$ with CTAB	BPM	CH_4	34	120	> 6	[2]
Ag foam	3 M $KHCO_3$	BPM	CO	59	100	3.6	[3]
Ag nanoparticles	3 M $KHCO_3$	BPM	CO	37	100	n/a	[4]
Ag nanoparticles	3 M $KHCO_3$	BPM	CO	82	100	n/a	[5]
Electrodeposited Bi	3 M $KHCO_3$	BPM	$HCOO^-$	64	100	> 4	[6]
Ag nanoparticles	2M MEA with 2M KCl	CEM	CO	72	50	− 0.8 vs. RHE	[7]

References

[1] Y. C. Li, G. Lee, T. Yuan, Y. Wang, D.-H. Nam, Z. Wang, F. P. García de Arquer, Y. Lum, C.-T. Dinh, O. Voznyy, E. H. Sargent, *ACS Energy Lett.* **2019**, *4*, 1427-1431.

[2] E. W. Lees, A. Liu, J. C. Bui, S. Ren, A. Z. Weber, C. P. Berlinguette, *ACS Energy Lett.* **2022**, 1712-1718.

[3] Z. Zhang, E. W. Lees, F. Habibzadeh, D. A. Salvatore, S. Ren, G. L. Simpson, D. G. Wheeler, A. Liu, C. P. Berlinguette, *Energy Environ. Sci.* **2022**, *15*, 705-713.

[4] T. Li, E. W. Lees, M. Goldman, D. A. Salvatore, D. M. Weekes, C. P. Berlinguette, *Joule* **2019**, *3*, 1487-1497.

[5] E. W. Lees, M. Goldman, A. G. Fink, D. J. Dvorak, D. A. Salvatore, Z. Zhang, N. W. X. Loo, C. P. Berlinguette, *ACS Energy Lett.* **2020**, *5*, 2165-2173.

[6] T. Li, E. W. Lees, Z. Zhang, C. P. Berlinguette, *ACS Energy Lett.* **2020**, *5*, 2624-2630.

[7] G. Lee, Y. C. Li, J.-Y. Kim, T. Peng, D.-H. Nam, A. Sedighian Rasouli, F. Li, M. Luo, A. H. Ip, Y.-C. Joo, E. H. Sargent, *Nat. Energy* **2021**, *6*, 46-53.